

Special
Issue

Towards Reproducible Fabrication of Nanometre-Sized Carbon Electrodes: Optimisation of Automated Nanoelectrode Fabrication by Means of Transmission Electron Microscopy

Patrick Wilde⁺,^[a] Thomas Quast⁺,^[a] Harshitha B. Aiyappa,^[a] Yen-Ting Chen,^[a] Alexander Botz,^[a] Tsvetan Tarnev,^[a] Miriam Marquitan,^[a] Stephan Feldhege,^[b] Armin Lindner,^[b] Corina Andronesu,^[a] and Wolfgang Schuhmann^{*[a]}

The reproducible fabrication of nanometre-sized carbon electrodes poses great challenges. Especially, the field of single entity electrochemistry has strict requirements regarding the geometry of these electrochemical probes. Herein, an automated setup for the fabrication of carbon nanoelectrodes based on the pyrolysis of a propane/butane gas mixture within pulled quartz capillaries by means of a moving heating coil is presented. It is

shown that mere electrochemical characterisation with conventional redox mediators does not allow for a reliable assessment of the electrode's geometry and quality. Therefore, high-throughput transmission electron microscopy is used in parallel to evaluate and optimise preparation parameters. Control of the latter gives access to three different electrode types: nanopipettes, nanosamplers and nanodisks.

1. Introduction

Electrochemistry at the nanoscale has embraced numerous fields of research ranging from the investigation of processes inside biological cells to the evaluation of functional materials in the shape of single nanoparticles.^[1] Studying underlying principles as well as extracting material properties at these dimensions poses great challenges to analytical tools and methods.^[2,3,4] The requirements for probes, which can help to elucidate scientific questions in the field of nano-research, can vary substantially depending on the specific field of application. Whereas factors like high sensitivity towards the analyte, stability and reliability are prerequisites of any probe, many systems have additional requirements. Biological samples, for instance, demand non-invasiveness due to their susceptibility towards physical damage,^[5] while the investigation of electrocatalysts requires the probe's inertness towards the catalytic reaction in order to avoid influence of the catalyst's intrinsic activity.

Over the past decades multiple types of nanosensors and nanoelectrodes have been developed for different applications. Owing to their small dimensions they are successfully employed

in single-entity electrochemistry.^[6] The electrochemical response of single nanoparticles^[2,3,7] and single molecules^[8] could be studied as well as physiologically relevant molecules inside living tissue and single living cells.^[9] Furthermore, the implementation into scanning electrochemical microscopy (SECM) laid the groundwork for high-resolution imaging of a nanostructured surface's reactivity and topography.^[10,11]

Different fabrication techniques have been employed to fabricate both metal- and carbon-based nanoelectrodes with defined geometry. Initially, inspired by scanning tunnelling microscopy (STM) tips, Pt/Ir alloy rods were electrochemically etched in acidic solution to yield nanometre-sized tips, which were subsequently insulated with glass or wax. The final nanoelectrodes were obtained by excavation of the apex.^[12] Another method used to obtain metal nanoelectrodes is achieved by pulling and sealing a metal wire inside a quartz capillary by means of a CO₂ laser puller. Exposition of the electrode's tip and a defined geometry is achieved through polishing.^[13] Due to their relative inertness towards electrocatalytic reactions, comparably low cost and ease of fabrication, carbon-based nanoelectrodes have recently attracted special attention. Two major approaches for their fabrication have emerged. One is based on the use of (flame)-etched carbon microfibers, which are pre-embedded in an insulating material.^[5,14] The other approach deploys the deposition of a carbonaceous layer on the inside of pulled quartz capillaries, by means of chemical vapour deposition (CVD). For this purpose either a classical CVD setup is used, typically with methane gas as a precursor,^[15] or pyrolysis of a propane/butane gas mixture in a pre-pulled, gas-filled quartz capillary is performed with a burner torch inside an argon counter-flow.^[11,16] The appeal of the latter method lies especially in its short electrode preparation time and the setup's inexpensiveness and simplicity.

[a] P. Wilde,⁺ T. Quast,⁺ H. B. Aiyappa, Y.-T. Chen, A. Botz, T. Tarnev, M. Marquitan, C. Andronesu, W. Schuhmann
Analytical Chemistry – Center for Electrochemical Sciences (CES), Ruhr-Universität Bochum, Universitätsstraße 150, D-44780 Bochum, Germany
E-mail: wolfgang.schuhmann@rub.de

[b] S. Feldhege, A. Lindner
Mechanical Workshop of the Faculty of Chemistry and Biochemistry, Ruhr-Universität Bochum, Universitätsstraße 150, D-44780 Bochum, Germany

[⁺] Authors contributed equally

Supporting information for this article is available on the WWW under <https://doi.org/10.1002/celc.201800600>

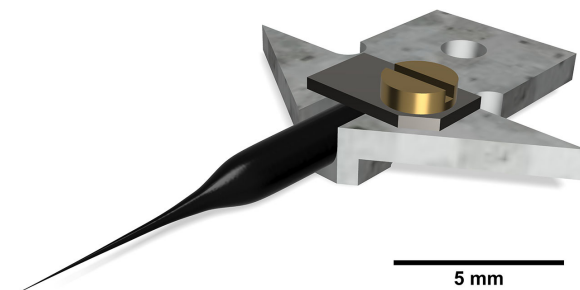
An invited contribution to a Special Issue on Single-Entity Electrochemistry

In this context, variations of CVD parameters lead to different electrode geometries. Apart from the conventional nanodisk shape, nanometre-sized pipettes with a thin carbon film on the inner wall could be obtained as well as carbon nanosamplers, which exhibit a nanocavity adjacent to the tip of the electrode.^[17,18] These specialised electrode configurations are exploited to facilitate novel types of experiments in which, for instance, the current response and physical properties of single captivated nanoparticles were investigated,^[19] or single particles were specifically delivered to electrified interfaces.^[20] Considering the vast and diverse application field for these types of nanoprobe, a reproducible fabrication method and reliable characterisation is highly imperative. Conventionally, characterisation of the effective electroactive surface area is performed via potentiodynamic cycling of the electrode in solution containing fast diffusing redox mediators. Predominantly, aqueous potassium chloride solutions with 1,1'-ferrocenedimethanol (Fc_{di}MeOH) or [Ru(NH₃)₆]^{3+/2+} (Ruhex) are used for this purpose.^[21] In the case of nanometre-sized Pt and Ag electrodes, however, it was shown, that unambiguous determination of the real electrode geometry by its voltammetric response is aggravated due to uncertainty in its shape.^[22]

Here, we demonstrate that mere knowledge of the electrochemically active surface area of nanometre-sized carbon electrodes does not provide sufficient information to estimate the quality of a produced electrode and distinguish between different geometries. To enable high-resolution imaging, a novel electrode holder, which allows for high-throughput transmission electron microscopy (TEM) of the nanoprobe is designed. We show that rigorous TEM analysis can substantially contribute to the understanding of the influence of the preparation parameters on the quality and geometry of the final electrode. To ensure a higher degree of control over these parameters a novel pyrolysis setup for the preparation of nanometre-sized carbon electrodes is introduced. It makes use of an electric heating coil instead of a conventional burner torch and includes extensive automatisisation. Most importantly variations of parameters and the setup are found to produce three different electrode geometries: nanodisks, nanopipettes and nanosamplers.

2. Results and Discussion

The use of the voltammetric response of fast diffusing redox mediators like Fc_{di}MeOH or Ruhex to reliably assess the quality and characteristics of a prepared nanometre-sized carbon electrode is investigated. For this purpose, a complementary microscopic method is used. Since most techniques cannot operate at the nanoscale dimensions of the tip, transmission electron microscopy (TEM) is the most powerful tool to provide the desired information. In general practice, the nanoelectrode tip is cut off and eventually glued to a conventional TEM grid with a vacuum resistant glue.^[17,18] The major drawbacks of this cumbersome method, however, is the required precision to place the tip in such a way, that the apex can be found in one of the grid's electron penetrable holes and can be positioned in



Scheme 1. Custom-made electrode holder for TEM. Total electrode length is 12 mm with a maximum diameter of 1.2 mm. Holder size is below 1 cm in all dimensions. The main body is made of vacuum-grade aluminium, the platelet of stainless steel and the screw's material is brass.

the focal plane of the electron beam as well as the fact, that the respective tip cannot be used for follow-up experiments anymore.

To circumvent these limitations a custom-made electrode holder was developed that could be mounted on a sample holder, which is compatible with the Jeol JEM-2800 transmission electron microscope (Scheme 1). In order to mount the electrode on the holder, the tip only needs to be cut to a total length of 12 mm, inserted and fixed in position. The advantage of this method does not only lie in the short preparation time but especially in the fact, that the tip can be removed from the holder after TEM imaging and still be used for follow-up (electrochemical) investigations that can go beyond basic electrode characterisation. This opens up the possibility to perform identical location TEM of nanomaterials, which are immobilised on nanometre-sized carbon electrodes. Three types of electrodes were prepared using various preparation procedures, to obtain different electrode geometries. Initial characterisation in Ruhex yielded very similar results (Figure 1d). In fact, the diffusion limited steady-state currents of -127 pA, -132 pA and -134 pA suggest almost identical electrodes, if a hemi-spherical diffusion field is assumed for all cases. Only subsequent TEM analysis revealed, that the electrode geometries and quality varied significantly between a disfigured tip (Figure 1a), a recessed tip (Figure 1b) and a hollow nanopipette with a thin carbon film on the inside (Figure 1c). This observation underlines, that performing only electrochemical characterisation can lead to incorrect conclusions due to the shape uncertainty of nanometre-sized carbon electrodes.

At scan rates above $50 \text{ mV} \cdot \text{s}^{-1}$ recessed carbon nanoelectrodes with an approximate orifice diameter of 100 nm were reported to exhibit behaviour, similar to that of thin layer cells.^[18] Slightly asymmetric peaks were observed, which increased prominently at higher scan rates. The peaks were attributed to the complete consumption of redox mediator molecules inside of a confined nanovolume, which cannot be replenished in the time scale of the experiment.

In order to investigate the use of variations of the scan rate or the nature of the redox mediators to potentially unveil the geometry and quality of slightly larger electrodes without the use of TEM, cyclic voltammograms were recorded in Ruhex and Fc_{di}MeOH with scan rates between $25 \text{ mV} \cdot \text{s}^{-1}$ and $1000 \text{ mV} \cdot \text{s}^{-1}$

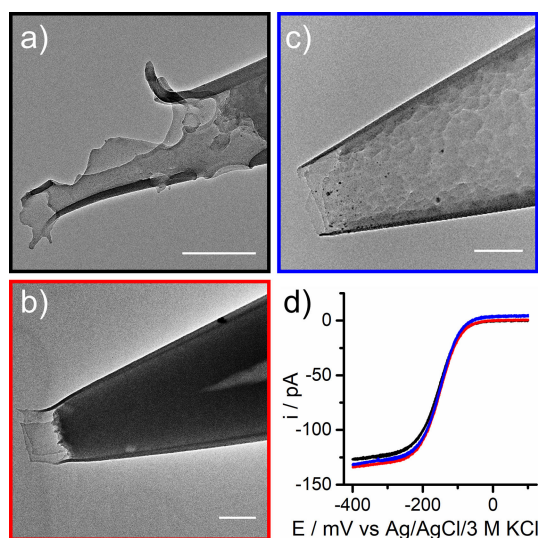


Figure 1. TEM images of three different electrode types, disfigured (a), recessed (b) and hollow nanopipette (c). Electrochemical response of the three electrode types in Ruhex, measured at a scan rate of $25 \text{ mV} \cdot \text{s}^{-1}$. Scale bar equals 200 nm in all cases. Colour code indicates cyclic voltammograms in (d).

(Figure 2). For this purpose, an electrode with a large recess and partial closure of the tip was chosen, which exhibited an orifice diameter of approximately 200 nm (Figure S1). Both sets of voltammograms exhibit identical current responses respectively, regardless of the scan rate. Considering the different diffusion coefficients of Ruhex and FcdiMeOH, both systems provide similar electrochemical information (see SI for more information).

However, none of the curves show the expected peak due to mass transport limitation through the orifice of the electrode. Thus, the recess of this specific electrode remains unrevealed by means of conventional electrochemical characterisation. An additional example is given in the SI (Figure S2).

These observations underline once more the necessity of TEM imaging in conjunction with electrochemical characterisation for the evaluation and optimisation of parameters for the nano-electrode fabrication process. It has to be noted that electrode preparation by means of pyrolysis of a propane/butane gaseous

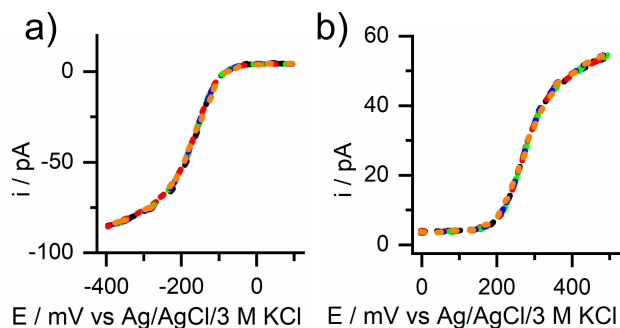


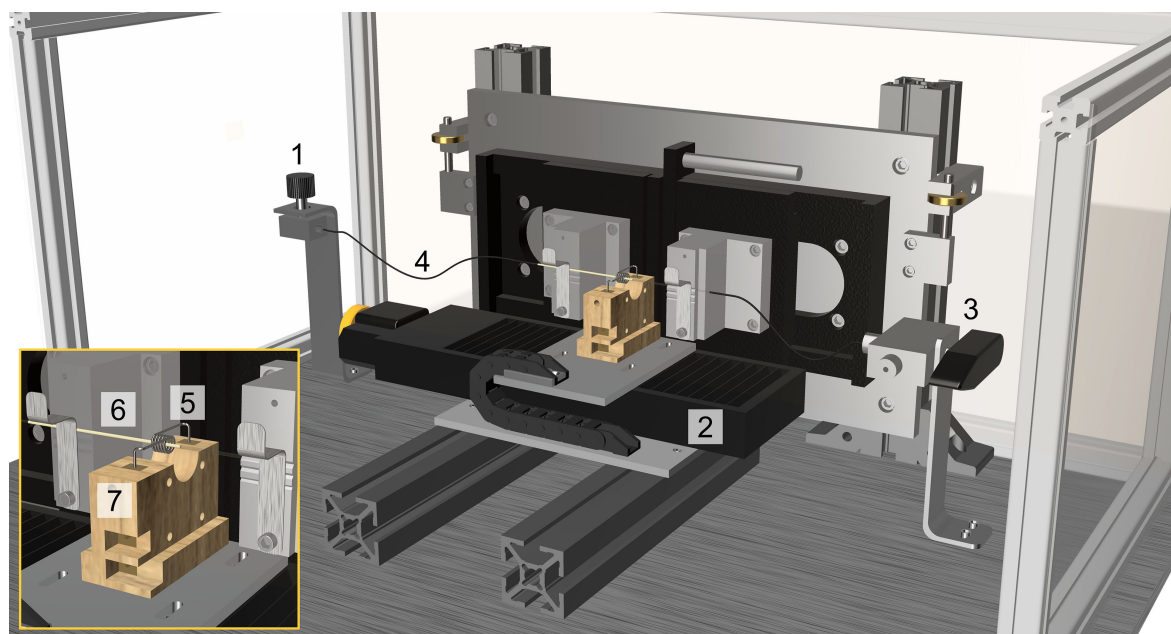
Figure 2. Cyclic voltammograms of the identical electrode in Ruhex (a) and FcdiMeOH (b) at different scan rates: $25 \text{ mV} \cdot \text{s}^{-1}$ (black), $50 \text{ mV} \cdot \text{s}^{-1}$ (red), $100 \text{ mV} \cdot \text{s}^{-1}$ (blue), $500 \text{ mV} \cdot \text{s}^{-1}$ (green) and $1000 \text{ mV} \cdot \text{s}^{-1}$ (orange). Graphs are dotted for better visibility.

mixture inside a pulled quartz capillary with a handheld burner torch has a major and critical drawback, despite its obvious advantages like short preparation times and simplicity of the setup. The shortcoming lies in the inability to precisely control the flame movement by hand as well as the flame temperature. The latter does not only depend on the burner gas pressure but also on the distance between capillary and flame and can therefore be hardly controlled. Hence, results can significantly differ in terms of geometry within one set of prepared electrodes (Figure S3). In order to provide a stricter parameter control, a novel electrode preparation setup was designed (Scheme 2).

Based on an approach described in literature^[11,23] the setup was evolved around the use of a heating coil instead of a gas flame to initiate pyrolysis inside the quartz capillary. The temperature of the coil, which acts as a heating resistor, can be precisely tuned by controlling the current flowing through it. Due to its high thermal stability with a recommended maximum temperature of 1330°C and its specific resistance of $1.39 \Omega \cdot \text{mm}^2 \cdot \text{m}^{-1}$ a CrFeAl alloy wire (22/73/5 wt.%) with a 1 mm cross-sectional diameter was used. The heating coil is mounted on top of a step-motor driven stage and both, heating current as well as coil movement can be controlled synchronously via a computer, thus minimising human inaccuracy. In order to centre the quartz and the argon counter-flow capillary inside the heating coil their position can be finely tuned in vertical and horizontal direction.

The rate of the argon flow through the Al_2O_3 counter-flow capillary is controlled by means of a pressure regulator and a needle valve. A three-way valve controls the feeder gas mixture of propane and butane, the pressure of which is adjusted by two individual pressure regulators. A more detailed description of the pyrolysis procedure is included in the experimental section. Prior to pyrolysis, different fabrication protocols were programmed. They determine the moving sequences of the coil and the velocity, with which its movement is executed (Figure S4a) as well as the applied heating current. Subsequently, temperature profiles were recorded during movement of the heated coil by introduction of a K-type thermoelement (Figure S4b) inside the argon counter-flow capillary. The tip of this sensor mimics the tip of the pulled quartz capillary. Regular adjustment of the heating current was used to ensure reproducible heating profiles, considering the limited life-time of the heating coil. TEM analysis and optical microscopy of pulled quartz capillaries revealed that their dimensions can vary despite using the same pulling parameters. The diameter of the orifice averages out at $223 \text{ nm} \pm 35 \text{ nm}$ ($n = 35$). The portion of the pre-pulled quartz capillary, which extends into the counter-flow capillary was found to vary by some hundreds of micrometres in length (average length equals $4720 \mu\text{m} \pm 170 \mu\text{m}$ for $n = 53$).

The starting position for the coil movement was adjusted with respect to the length of the heat sensor, to ensure similar heating profiles for capillaries of differing lengths. The first family of tips, that was produced, are nanopipettes, which are characterised by a thin carbon film on the inside of the quartz capillary and a free channel along the central axis of the electrode. For this purpose, a heating profile was used, which exhibits a steep incline in temperature before a plateau was



Scheme 2. Drawing of the pyrolysis setup. Inset is a magnification of the setup's central part. The main features are: 1) needle valve for regulation of the argon flow rate; 2) step-motor for coil movement; 3) three-way valve for mixing of precursor gases; 4) gas-tight rubber tubes; 5) CrFeAl alloy heating resistor coil; 6) ceramic argon counter-flow capillary containing the pulled quartz glass pipette; 7) Bakelite® support for heating coil.

reached at 960 °C for 35 s prior to cooling down for approximately 2 min (Figure 3a, black curve). The resulting electrode shows the characteristic carbon architecture of a nanopipette with an approximate carbon layer thickness of 90 nm and a minimum channel diameter of 120 nm (Figure 3b).

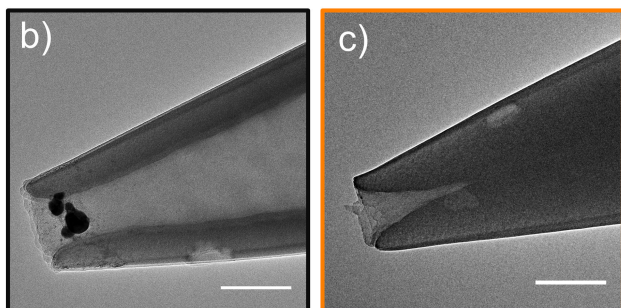
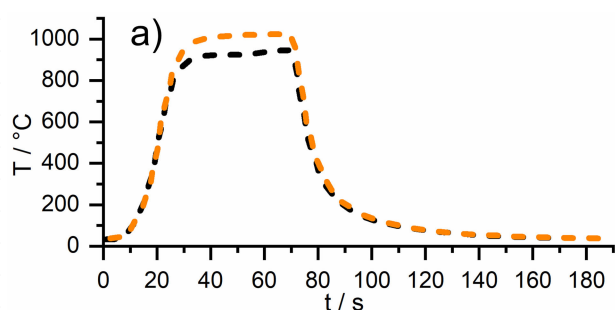


Figure 3. Temperature profiles for the preparation of nanopipettes (black) and nanosamplers (orange) (a). TEM images of (b) a nanopipette and (c) a nanosampler. Dark spots are dried crystals of KCl containing traces of ruthenium salts, which remained from electrochemical characterisation in Ruhex. Scale bars equal 200 nm.

In order to close the channel of the as-fabricated nanopipettes and obtain nanosamplers with a cone-shaped cavity directly adjacent to the apex, a similar heat profile was run. The plateau temperature was increased to 1020 °C (Figure 3a, orange curve) to promote enhanced deposition of the carbonaceous layer. Indeed, the resulting electrode (Figure 3c) exhibits the previously described carbon geometry of a nanosampler with an orifice diameter of 200 nm and a cavity depth of 325 nm. Additionally, the influence of a gradual temperature increase on the carbon layer thickness was further investigated and more information can be found in the supporting information (Figure S5). For the preparation of nanometre-sized carbon disk electrodes a more sophisticated two-step heating profile was applied (Figure 4a). In the first step (pre-pyrolysis) a rapid temperature increase to 960 °C is used to form a thin conductive layer of carbon on the inside of the quartz glass walls, similar to the fabrication of nanopipettes. Subsequently, the electrode is cooled down to 100 °C and a second heating step (post-pyrolysis) up to 700 °C followed by a gradual temperature decrease until approximately 460 °C facilitates the closure of the remaining orifice. Electrochemical characterisation of the resulting electrode in Ruhex solution yields a diffusion limited steady-state current of 222 pA at -400 mV vs Ag/AgCl/3 M KCl. However, only the TEM image of the final electrode (Figure 4b) reliably reveals the electrode nanodisk geometry. Moreover, it provides evidence for the abovementioned carbon formation process. Areas of higher contrast are observable starting approximately 200 nm from the tip, which resemble a thin carbon film that is expected to form during pre-pyrolysis. During post-pyrolysis this film becomes denser and hence higher in TEM contrast, whereas the remaining volume is also filled with carbon of lower density. EDS mapping provides evidence, that the quartz apex (red signifies silicon) is

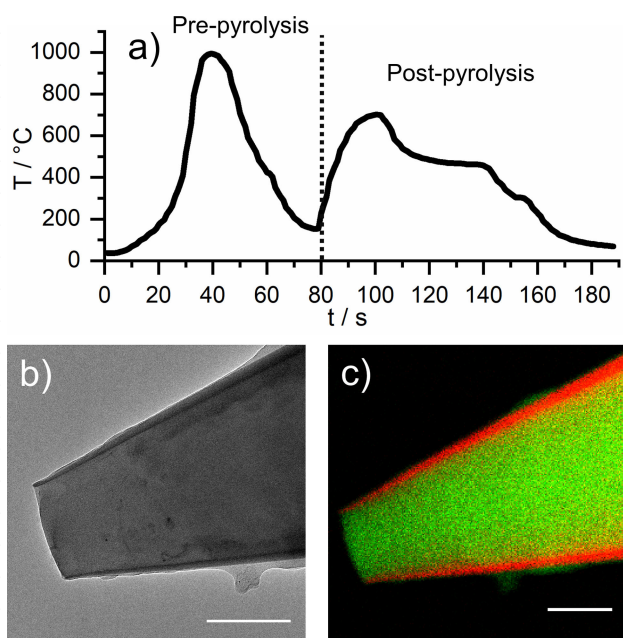


Figure 4. Temperature profile for the preparation of nanometre-sized carbon disk electrodes (a). TEM image of a nanometre-sized carbon electrode with disk geometry (b) and energy-dispersive X-ray spectroscopy (EDS) (c) mapping of the same electrode. Green indicates the presence of carbon and red corresponds to silicon. Scale bars equal 200 nm.

otherwise homogeneously filled with carbon (green). Omission of the pre-pyrolysis step led to electrically non-connectable electrodes, underlining the importance of the heating profile for the resulting electrode. Moreover, this observation shows, that precise parameter control and access to more sophisticated pyrolysis procedures open up new ways for electrode design. Additional examples for each electrode type can be found in Figure S6.

Small variations in the temperature profiles during the post-pyrolysis step (see Figure S7) indicate that the formation of an ideal nanometre-sized disk is the result of a sensitive equilibrium between a carbon overgrowth at the electrode tip at lower temperatures (Figure 5a) and the burning away of the carbon due to traces of oxygen left in the system at increased temperatures (Figure 5b). Hence, strict parameter control, especially regarding the temperature at the tip of the electrode,

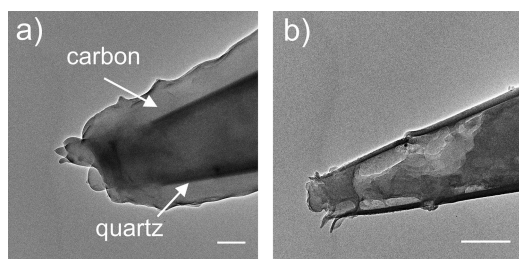


Figure 5. TEM images of electrodes prepared via the two-step approach. Temperature variations in the post-pyrolysis step lead to overgrown electrodes at lower temperatures (a) and to burnt electrodes at higher temperatures (b). Scale bars equal 200 nm.

appears to be imperative for the reproducible fabrication of disk-shaped nanometre-sized carbon electrodes.

3. Conclusions

The reliable assessment of the geometry and quality of nanometre-sized carbon electrodes is impossible solely by the use of electrochemical characterisation. TEM is used as a powerful tool for the investigation of electrode characteristics. Strict parameter control and parallel use of high-throughput TEM is proposed to facilitate optimisation of the fabrication parameters. Fabrication of nanometre-sized carbon electrodes can be realised by means of a heating coil, which replaces the conventional burner torch flame. The proposed extensive automatization provides improved control over the heating profile during pyrolysis. Accurate coil positioning and current control allows to apply sophisticated fabrication protocols. In this context, two-step pyrolysis gives access to the envisaged nanodisk geometry. Even slight variations of this profile were shown to have a significant effect on the geometry and quality of the fabricated electrode. Ultimately, this correlation gives access to three different electrode families: nanopipettes, nano-samplers and disk-shaped nanometre-sized carbon electrodes. Further parameter optimisation and the investigation of alternative fabrication protocols will be performed in the future to allow for a facilitated fabrication of nanometre-sized, disk-shaped carbon electrodes, which allows for a wider margin of preparation parameters.

Experimental Section

The basic framework of the pyrolysis setup is widely custom-made. Ceramic argon counter-flow capillaries (*Friatec*) have a nominal inner diameter of 0.8 mm and an outer diameter of 1.2 mm. The CrFeAl alloy wire (22/73/5 wt.%) (*Berghütten*) was cleaned with acetone before a custom-made instrument was used to reproducibly form heating coils. The step-motor was acquired from *OWIS* and the precision needle valve for the argon counter-flow was bought from *HOKE*. Gas lines were constructed using standard stainless-steel pipes and screw joints of *Swagelok*. The three-way valve for the pyrolysis gas mixture was also purchased from *Swagelok*. Pressure regulators (*Vulkan*) were directly attached to the gas bottles. A direct-current power supply (*Voltcraft* SPS-1560-PFC) was used to control the heating current. Heating profiles were recorded with a K-type thermoelement (*Omega*) in combination with a multi-meter (*CEM* DT-9939). A gas-tight rubber tube (*RCT Reichelt Chemietechnik*) was used for the connection between the *Swagelok* gas system and the capillaries. Quartz capillaries (*Sutter Instruments*) with 0.9 mm inner diameter and a 1.2 mm outer diameter were cleaned with ultrasonication treatment in acetone for 15 min and pulled by using a *Sutter Instruments* P-2000 laser puller. Typical pulling parameters were HEAT = 720, FILAMENT = 4, VELOCITY = 45, DELAY = 130 and PULL = 100. During pyrolysis the Ar counter-flow (*Air Liquide*, 99.999%) was set at a rate of $53 \text{ mL} \cdot \text{min}^{-1}$ with the Ar pressure fixed at 0.5 bar. Pyrolysis gas was introduced as a mixture of propane (*Air Liquide*, technical grade) with a pressure of 3 bar and n-butane (*Air Liquide*, 99.5%) with a pressure of 1.1 bar. Coil movement and heating current were simultaneously controlled by an in-house programmed software. After pyrolysis, the electrode was allowed to cool down under Ar

stream for at least additional 35 s to prevent burning away of carbon under atmospheric conditions. Electrochemical characterisation was performed inside a Faraday cage using a VA-10 voltammetric amplifier (*npi*) in a two-electrode setup. An Ag/AgCl/3 M KCl electrode served as reference and counter electrode. Redox mediator solutions were prepared using 1,1'-ferrocenedimethanol or $[\text{Ru}(\text{NH}_3)_6]^{3+/2+}$ (both *Sigma Aldrich*) with a concentration of 5 mM in 0.1 M KCl (*J.T. Baker*) solution. Chemicals were used as received. Water was deionised employing a water purification system (SG) to obtain conductivities of less than $0.055 \mu\text{S}\cdot\text{cm}^{-1}$. High resolution transmission electron microscopy (HRTEM) was performed on a JEOL microscope (JEM-2800) with a Schottky-type emission source working at 200 kV, equipped with a Gatan OneView camera ($4k\times 4k$, 25FPS). The resolution of the TEM images is 0.09 nm. Energy dispersive spectroscopy (EDS) mapping was performed with the equipped double SDD detectors, with a solid angle of 0.98 steradians with a detection area of 100 mm^2 .

Acknowledgements

The authors are grateful to the Deutsche Forschungsgemeinschaft in the framework of the Forschergruppe (FOR 2397-1; SCHU 929/15-1) "Multi-scale analysis of complex three-phase systems: oxygen reduction on gas-diffusion electrodes in aqueous electrolyte" and the Cluster of Excellence "Resolv" (EXC1069). J. Clausmeyer, T. Löffler and D. Öhl are acknowledged for helpful discussions. P.W. is grateful to the Association of the Chemical Industry e.V. (VCI) for funding of the PhD fellowship.

Conflict of Interest

The authors declare no conflict of interest.

Keywords: electrode fabrication • electron microscopy • nanometre-sized carbon electrodes • nanotechnology • setup automatisation

- [1] S. M. Oja, Y. Fan, C. M. Armstrong, P. Defnet, B. Zhang, *Anal. Chem.* **2016**, *88*, 414.
- [2] J. Clausmeyer, W. Schuhmann, *Trends. Anal. Chem.* **2016**, *79*, 46.
- [3] K. McKelvey, S. R. German, Y. Zhang, H. S. White, M. A. Edwards, *Curr. Opin. Electrochem.* **2017**, *6*, 4.
- [4] a) Y.-L. Ying, Z. Ding, D. Zhan, Y.-T. Long, *Chem. Sci.* **2017**, *8*, 3338; b) Y. Takahashi, Y. Zhou, T. Fukuma, *Curr. Opin. Electrochem.* **2017**, *5*, 121.
- [5] Y.-T. Li, S.-H. Zhang, L. Wang, R.-R. Xiao, W. Liu, X.-W. Zhang, Z. Zhou, C. Amatore, W.-H. Huang, *Angew. Chem. Int. Ed.* **2014**, *53*, 12456.
- [6] a) S. Chen, Y. Liu, *Phys. Chem. Chem. Phys.* **2014**, *16*, 635; b) M. V. Mirkin, T. Sun, Y. Yu, M. Zhou, *Acc. Chem. Res.* **2016**, *49*, 2328.
- [7] a) Y. Yu, Y. Gao, K. Hu, P.-Y. Blanchard, J.-M. Noël, T. Nareshkumar, K. L. Phani, G. Friedman, Y. Gogotsi, M. V. Mirkin, *ChemElectroChem* **2015**, *2*, 58; b) Y. Li, J. T. Cox, B. Zhang, *J. Am. Chem. Soc.* **2010**, *132*, 3047; c) J.

- Clausmeyer, J. Masa, E. Ventosa, D. Öhl, W. Schuhmann, *Chem. Commun.* **2016**, *52*, 2408.
- [8] a) J. C. Byers, B. Paulose Nadappuram, D. Perry, K. McKelvey, A. W. Colburn, P. R. Unwin, *Anal. Chem.* **2015**, *87*, 10450; b) L. Han, W. Wang, J. Nsabimana, J.-W. Yan, B. Ren, D. Zhan, *Faraday Discuss.* **2016**, *193*, 133.
- [9] a) M. Marquitan, J. Clausmeyer, P. Actis, A. L. Córdoba, Y. Korchev, M. D. Mark, S. Herlitze, W. Schuhmann, *ChemElectroChem* **2016**, *3*, 2125; b) Y. Liu, M. Li, F. Zhang, A. Zhu, G. Shi, *Anal. Chem.* **2015**, *87*, 5531; c) H. R. Rees, S. E. Anderson, E. Privman, H. H. Bau, B. J. Venton, *Anal. Chem.* **2015**, *87*, 3849.
- [10] a) B. Ballesteros Katemann, A. Schulte, W. Schuhmann, *Electroanalysis* **2004**, *16*, 60; b) M. A. O'Connell, J. R. Lewis, A. J. Wain, *Chem. Commun.* **2015**, *51*, 10314; c) M. A. O'Connell, A. J. Wain, *Anal. Chem.* **2014**, *86*, 12100; d) M. Kang, D. Momotenko, A. Page, D. Perry, P. R. Unwin, *Langmuir* **2016**, *32*, 7993; e) B. P. Nadappuram, K. McKelvey, J. C. Byers, A. G. Güell, A. W. Colburn, R. A. Lazenby, P. R. Unwin, *Anal. Chem.* **2015**, *87*, 3566; f) T. Kai, C. G. Zoski, A. J. Bard, *Chem. Commun.* **2018**, *54*, 1934; g) Y. Takahashi, H. Ida, Y. Matsumae, H. Komaki, Y. Zhou, A. Kumatani, M. Kanzaki, H. Shiku, T. Matsue, *Phys. Chem. Chem. Phys.* **2017**, *19*, 26728.
- [11] Y. Takahashi, A. I. Shevchuk, P. Novak, Y. Zhang, N. Ebejer, J. V. Macpherson, P. R. Unwin, A. J. Pollard, D. Roy, C. A. Clifford, *Angew. Chem. Int. Ed.* **2011**, *50*, 9638.
- [12] a) R. M. Penner, M. J. Heben, T. L. Longin, N. S. Lewis, *Science* **1990**, *250*, 1118; b) L. A. Nagahara, T. Thundat, S. M. Lindsay, *Rev. Sci. Instrum.* **1989**, *60*, 3128.
- [13] a) Y. Li, D. Bergman, B. Zhang, *Anal. Chem.* **2009**, *81*, 5496; b) B. B. Katemann, W. Schuhmann, *Electroanalysis* **2002**, *14*, 22; c) N. Nioradze, R. Chen, J. Kim, M. Shen, P. Santhosh, S. Amemiya, *Anal. Chem.* **2013**, *85*, 6198.
- [14] a) T. G. Strein, A. G. Ewing, *Anal. Chem.* **1992**, *64*, 1368; b) X. Li, S. Majdi, J. Dunevall, H. Fathali, A. G. Ewing, *Angew. Chem. Int. Ed.* **2015**, *54*, 11978; c) K. T. Kawagoe, J. A. Jankowski, R. M. Wightman, *Anal. Chem.* **1991**, *63*, 1589.
- [15] a) M. G. Schrlau, E. M. Falls, B. L. Ziober, H. H. Bau, *Nanotechnology* **2008**, *19*, 15101; b) R. Singhal, S. Bhattacharyya, Z. Orynbayeva, E. Vitol, G. Friedman, Y. Gogotsi, *Nanotechnology* **2010**, *21*, 15304; c) E. A. Vitol, M. G. Schrlau, S. Bhattacharyya, P. Ducheyne, H. H. Bau, G. Friedman, Y. Gogotsi, *Chem. Vap. Deposition* **2009**, *15*, 204.
- [16] a) Y. T. Kim, D. M. Scamulis, A. G. Ewing, *Anal. Chem.* **1986**, *58*, 1782; b) M. McNally, D. K. Y. Wong, *Anal. Chem.* **2001**, *73*, 4793; c) J. Clausmeyer, P. Wilde, T. Löffler, E. Ventosa, K. Tschulik, W. Schuhmann, *Electrochem. Commun.* **2016**, *73*, 67; d) B. P. Nadappuram, K. McKelvey, R. Al Botros, A. W. Colburn, P. R. Unwin, *Anal. Chem.* **2013**, *85*, 8070.
- [17] Y. Wang, D. Wang, M. V. Mirkin, *Proc. R. Soc. A* **2017**, *473*, 20160931.
- [18] Y. Yu, J.-M. Noël, M. V. Mirkin, Y. Gao, O. Mashtalir, G. Friedman, Y. Gogotsi, *Anal. Chem.* **2014**, *86*, 3365.
- [19] a) K. Hu, Y. Wang, H. Cai, M. V. Mirkin, Y. Gao, G. Friedman, Y. Gogotsi, *Anal. Chem.* **2014**, *86*, 8897; b) M. Zhou, Y. Yu, K. Hu, H. L. Xin, M. V. Mirkin, *Anal. Chem.* **2017**, *89*, 2880.
- [20] K. McKelvey, M. A. Edwards, H. S. White, *J. Phys. Chem. Lett.* **2016**, *7*, 3920.
- [21] a) I. Agyekum, C. Nimley, C. Yang, P. Sun, *J. Phys. Chem. C* **2010**, *114*, 14970; b) R. Chen, K. Hu, Y. Yu, M. V. Mirkin, S. Amemiya, *J. Electrochem. Soc.* **2016**, *163*, H3032–H3037.
- [22] Y. Shao, M. V. Mirkin, G. Fish, S. Kokotov, D. Palanker, A. Lewis, *Anal. Chem.* **1997**, *69*, 1627.
- [23] F.-R. F. Fan, C. Demaille in *Scanning electrochemical microscopy* (Eds.: A. J. Bard, M. V. Mirkin), CRC Press, Boca Raton, Fla., **2012**, pp. 25–55.

Manuscript received: May 7, 2018

Accepted Article published: June 3, 2018

Version of record online: June 20, 2018